

The effects of flux transport on interface dynamos

J. Mason,^{1,2*} D.W. Hughes¹ and S.M. Tobias¹

¹*Department of Applied Mathematics, University of Leeds, Leeds LS2 9JT, UK*

²*Department of Astronomy and Astrophysics, University of Chicago, Chicago, IL 60637, USA*

6 November 2018

The definitive version is available at www.blackwell-synergy.com

ABSTRACT

The operation of an interface dynamo (as has been suggested for the Sun and other stars with convective envelopes) relies crucially upon the effective transport of magnetic flux between two spatially disjoint generation regions. In the simplest models communication between the two regions is achieved solely by diffusion. Here we incorporate a highly simplified anisotropic transport mechanism in order to model the net effect of flux conveyance by magnetic pumping and by magnetic buoyancy. We investigate the influence of this mechanism on the efficiency of kinematic dynamo action. It is found that the effect of flux transport on the efficiency of the dynamo is dependent upon the spatial profile of the transport. Typically, transport hinders the onset of dynamo action and increases the frequency of the dynamo waves. However, in certain cases there exists a preferred magnitude of transport for which dynamo action is most efficient. Furthermore, we demonstrate the importance of the imposition of boundary conditions in drawing conclusions on the role of transport.

Key words: MHD – Sun: activity – Sun: magnetic fields

1 INTRODUCTION

The solar magnetic field is maintained by the action of a hydromagnetic dynamo. The well-known eleven year solar activity cycle corresponds to a twenty-two year magnetic cycle, the origin of which lies deep within the solar interior (see, for example, Charbonneau 2005). The key to understanding the generation of the solar magnetic field lies in establishing the form of both the large- and small-scale fluid flows in the interior. Helioseismology, the study of acoustic fluctuations within the Sun, has provided a map of the solar differential rotation (Schou et al. 1998), which shows that the surface latitudinal dependence is largely maintained throughout the convection zone while the solar interior rotates as a solid body. These two profiles are matched in a thin, stably stratified layer of strong differential rotation (shear) at the base of the convection zone – a region known as the tachocline. A discussion of the dynamics of the tachocline can be found in Tobias (2005) and Hughes, Rosner & Weiss (2007).

This region of pronounced shear is believed to be of paramount importance in the generation (via the so-called ω -effect), storage and eventual instability of a strong toroidal magnetic field. The regeneration of poloidal field from toroidal field is less well understood. It is typically ascribed to the α -effect of mean field electrodynamics, but the precise origin and location of this mechanism remain unclear. A number of possibilities have been suggested (see the review of Ossendrijver 2003). The most natural is to appeal to convective turbulence in the presence of rotation (Parker 1955; Steenbeck, Krause & Rädler 1966). There are however some difficulties for this approach both in the linear (Cattaneo & Hughes 2006, Hughes & Cattaneo 2008) and nonlinear regimes (see the reviews by Diamond, Hughes & Kim 2005; Brandenburg & Subramanian 2005). An alternative is to appeal to magnetic buoyancy instabilities of the tachocline field interacting with rotation (Schmitt, Schüssler & Ferriz-Mas 1996; Thelen 2000; see also Cline, Brummell & Cattaneo 2003 for a related model). A third possibility places the generation of poloidal field well away from the tachocline, the assumed location for the generation of toroidal field. In this paradigm (Dikpati & Charbonneau 1999; Dikpati & Gilman 2001) poloidal flux is regenerated via the decay of active regions

* E-mail: jmason@flash.uchicago.edu; d.w.hughes@leeds.ac.uk; smt@maths.leeds.ac.uk.

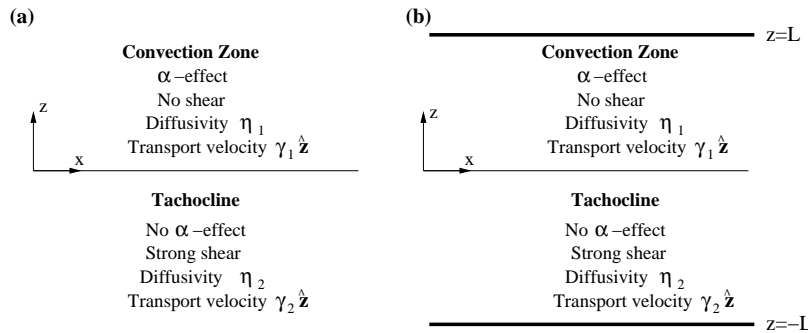


Figure 1. Geometry of the two models: (a) Model I, (b) Model II. We consider a local Cartesian geometry in the northern hemisphere, with the z -axis pointing radially outwards (upwards), the x -axis pointing towards the equator and the y -axis in the azimuthal direction. The models differ only by the z -extent of the domain.

at the solar surface (Babcock 1961; Leighton 1969). In these models meridional circulation is invoked in order to transport the new poloidal flux to the tachocline. This model too is not without difficulties (see the review by Tobias & Weiss 2007).

In this paper we shall consider models of dynamos operating at an interface between regions of turbulent rotating convection and velocity shear. The idea of an interface dynamo — with neighbouring regions of α - and ω -effects — was introduced by Parker (1993) expressly to avoid the difficulties caused by the strong suppression of turbulent magnetic diffusion by a weak mean field. In Parker’s model, strong toroidal field is generated in the tachocline by radial shear. There, and only there, does it suppress the diffusion, leading naturally to confinement of the toroidal field within that layer. The α -effect and a healthy turbulent diffusion operate relatively unimpeded in the bulk of the convection zone. Parker suggested that provided the diffusivity is not suppressed too strongly, observed solar fluxes and the 22-year solar period could be accommodated. Parker’s original kinematic model has been extended into the nonlinear regime to investigate explicitly the quenching not only of the turbulent diffusion but also of the α -effect (Tobias 1996; Charbonneau & MacGregor 1997; Markiel & Thomas 1999).

A crucial ingredient for efficient interface dynamo action is the transport of magnetic flux between the two spatially disjoint generation regions. For this reason, dynamo action is, typically, more difficult to excite in such models than in those with spatially-coincident generation mechanisms (Parker 1993). Indeed, if such a transport mechanism is absent, this places a severe constraint on the applicability of interface dynamos (Dikpati et al. 2005). Within the Sun there are however a number of possible mechanisms that could transport magnetic field. For example, convective pumping (e.g. Drobyshevski & Yuferev 1974) is believed to transport flux downwards from the convection zone into the tachocline (e.g. Tobias et al. 1998, 2001; Dorch & Nordlund 2001). Turbulent diffusion, which is believed to act throughout the convection zone but could be significantly reduced in the tachocline (Parker 1993), acts to reduce gradients in field. Mean flows, such as the meridional circulation (Choudhuri et al. 1995), which is observed to be polewards at and just below the solar surface but is undetermined at the base of the convection zone, will act to advect mean flux. The only transport mechanism that is unambiguously directed outwards is magnetic buoyancy, which is believed to play a key role in the emergence of active regions at the surface (see, for example, the reviews by Schüssler 2005 and Hughes 2007). These competing effects may occur on different timescales and depend on the local strength of magnetic field. Indeed, the general picture we have of the solar dynamo is of the field being confined and maintained at the base of the convection zone, with occasional eruptions.

In this paper we consider the effect of incorporating non-diffusive flux transport in an interface dynamo model. In keeping with the simple yet illustrative nature of Parker’s original model, we include magnetic transport via an effective velocity. Indeed, such a velocity arises naturally in mean field electrodynamics as the ‘ γ -effect’, resulting from the anti-symmetric part of the α -tensor (Rädler 1968). It should be noted that mean field electrodynamics is not without problems, particularly in the high magnetic Reynolds number regime applicable to the Sun. Nonetheless, our hope is that it is possible to capture some features of the interaction of generation, transport and diffusion of magnetic fields via a simple mean-field model.

In this paper we shall investigate the role of the γ -effect on the onset of the dynamo instability for two kinematic $\alpha\omega$ -dynamo models. A natural starting point is to extend Parker’s 1993 model, in which the interface separates two spatially unbounded regions. It is though important to consider the more realistic case of vertically bounded domains, which is the aim of our second model. In §2 we discuss those characteristics that are common to both models. The effect of introducing flux transport is investigated, for the two models, in §3 and §4. The possible implications for an interface dynamo in the Sun are discussed in §5.

2 FORMULATION OF THE PARKER INTERFACE DYNAMO

We consider the role of flux transport for two models of kinematic, $\alpha\omega$ -interface dynamos in a local Cartesian geometry (see Figure 1). The region $z > 0$ represents the convection zone (although there is no convection as such in our framework), wherein the α -effect generates the poloidal field and there is no ω -effect. The region $z < 0$ models the tachocline, where the radial shear regenerates the toroidal field (the ω -effect) and $\alpha = 0$. The assumption of axisymmetry translates to solutions that are independent of the azimuthal direction, y say, and we shall consider fields that are periodic in x .

The induction equation for the mean field \mathbf{B} takes the form (see, for example, Moffatt 1978)

$$\frac{\partial \mathbf{B}}{\partial t} = \nabla \times (\mathbf{U} \times \mathbf{B}) + \nabla \times \boldsymbol{\mathcal{E}} + \eta_0 \nabla^2 \mathbf{B}, \quad (1)$$

where \mathbf{U} represents the mean flow, η_0 is the molecular magnetic diffusivity, and $\boldsymbol{\mathcal{E}}$ is the mean electromotive force, which takes the form

$$\mathcal{E}_i = \alpha_{ij} B_j + \beta_{ijk} \frac{\partial B_j}{\partial x_k} + \dots \quad (2)$$

For simplicity we shall consider the effects of anisotropy only in the α_{ij} tensor, which we assume to take the form $\alpha_{ij} = \alpha \delta_{ij} - \epsilon_{ijk} \gamma_k$. We assume that $\beta_{ijk} = \beta \epsilon_{ijk}$; β is then a turbulent magnetic diffusivity. Equation (1) now becomes

$$\frac{\partial \mathbf{B}}{\partial t} = \nabla \times (\mathbf{U} \times \mathbf{B}) + \nabla \times (\boldsymbol{\gamma} \times \mathbf{B}) + \nabla \times (\alpha \mathbf{B}) - \nabla \times (\eta (\nabla \times \mathbf{B})), \quad (3)$$

in which $\eta = \beta + \eta_0$. We shall consider models in which η may take different constant values in $z > 0$ and $z < 0$; thus, for the purpose of deriving the jump relations below, we do not take η outside the derivative in the above equation.

The large-scale velocity \mathbf{U} is chosen to represent the radial shear of the tachocline. The effective velocity $\boldsymbol{\gamma}$ describes the radial non-diffusive transport of magnetic flux between the two layers. We therefore take

$$\mathbf{U} = U(z) \hat{\mathbf{y}}, \quad \boldsymbol{\gamma} = \gamma(z) \hat{\mathbf{z}}, \quad (4)$$

where $dU/dz = GH(-z)$, $\gamma(z) = \gamma_2 + (\gamma_1 - \gamma_2)H(z)$ and $H(z)$ is the Heaviside function. Here G , γ_1 and γ_2 are constants. We may think of the situation in which $\gamma_i < 0$ ($i = 1, 2$) as the case in which magnetic pumping is the prevailing transport mechanism leading to a net transport radially inwards, while the case in which the dominant transport effect is by magnetic buoyancy (and hence directed radially outwards) is modelled by $\gamma_i > 0$.

As the system is axisymmetric (y -independent), it is useful to decompose the field into poloidal and toroidal parts, $\mathbf{B}(x, z, t) = \nabla \times A \hat{\mathbf{y}} + B \hat{\mathbf{y}}$. We proceed with the convention that subscripts 1 and 2 refer to quantities in $z > 0$ and $z < 0$, respectively. Assuming that the shear is much stronger than the α -effect in generating the toroidal field (the $\alpha\omega$ -approximation), it follows from equation (3) that in $z > 0$ the governing equations are

$$\frac{\partial A_1}{\partial t} = \alpha B_1 + \eta_1 \nabla^2 A_1 - \gamma_1 \frac{\partial A_1}{\partial z}, \quad \frac{\partial B_1}{\partial t} = \eta_1 \nabla^2 B_1 - \gamma_1 \frac{\partial B_1}{\partial z}, \quad (5)$$

while in $z < 0$ we have

$$\frac{\partial A_2}{\partial t} = \eta_2 \nabla^2 A_2 - \gamma_2 \frac{\partial A_2}{\partial z}, \quad \frac{\partial B_2}{\partial t} = \eta_2 \nabla^2 B_2 + G \frac{\partial A_2}{\partial x} - \gamma_2 \frac{\partial B_2}{\partial z}. \quad (6)$$

In both regions we seek wave-like solutions of the form

$$A = \Re[a(z)e^{pt+ikx}], \quad B = \Re[b(z)e^{pt+ikx}], \quad (7)$$

where $p = \sigma + i\omega$ ($\sigma, \omega \in \Re$), k is the wavenumber ($k > 0$), and $a(z)$ and $b(z)$ are the (complex) amplitudes of the dynamo waves. Temporally growing solutions ($\sigma > 0$), with period $T = 2\pi/\omega$, propagate equatorwards when $\omega < 0$ and towards the north pole when $\omega > 0$. Both A and B are continuous. The solutions are matched at the interface $z = 0$ by the jump conditions (derived by integrating equation (3) across the interface)

$$\left[\frac{\partial A}{\partial z} \right]_0 = 0, \quad \left[\eta \frac{\partial B}{\partial z} - \gamma B \right]_0 = 0, \quad (8)$$

where $[\cdot]_0$ denotes the jump in the specified quantity across $z = 0$. Applying the boundary conditions in z , which will be described later, leads to a dispersion relation connecting the growth rate and wavenumber to the non-dimensional dynamo number (D , say), which measures the relative strength of induction to diffusion. As the definition of D differs between the two models, we postpone its definition to the later sections.

To set the scene we now describe the spatial form of the transport mechanisms that we implement. As already described, the efficiency of an interface dynamo is crucially reliant on flux transport between the two generation layers. In Parker's model transport is solely by diffusion, with, in the simplest case, $\eta_1 = \eta_2$. The intention of Parker's model was to show how a strong field could be confined to a thin layer beneath the convection zone owing to that field suppressing the effective diffusion, leading to $\eta_2 \ll \eta_1$. We shall therefore investigate the role of the γ -effect in models with uniform diffusion ($\eta_1 = \eta_2$) and in those with $\eta_2/\eta_1 \ll 1$. We will consider the following illustrative cases:

- **Bidirectional transport with uniform diffusion**

We consider first the case in which $\gamma_1 = -\gamma_2 = \gamma$ with $\gamma < 0$, modelling pumping in $z > 0$ and magnetic buoyancy in $z < 0$.

For simplicity we take $\eta_1 = \eta_2$. Although one might expect stronger transport to increase the efficiency of the dynamo, we will show that this is not necessarily the case. We will then compare these results with the situation $\gamma > 0$, which represents flux transport away from the interface in both generation layers and hence may naively be expected to yield the least efficient dynamo.

- **Unidirectional transport with uniform diffusion**

Next we consider $\gamma_1 = \gamma_2 = \gamma$ and $\eta_1 = \eta_2$. We may think of $\gamma < 0$ as the typical solar case in which transport inwards by convective overshoot is expected to dominate the buoyant rise of magnetic field.

- **Dominant transport in the convection zone**

Here we assume that the net transport is much stronger in $z > 0$ and that effects due to magnetic buoyancy in $z > 0$ are small in comparison with convective transport. We therefore consider $\gamma_2 = 0$ and investigate the effects of increasing the magnitude of $\gamma_1 < 0$. This is motivated by what is believed to be the case at the base of the solar convection zone. We compare the case $\eta_2 = \eta_1$ with the more relevant case $\eta_2 \ll \eta_1$.

For chosen values of the γ -effect and diffusion coefficients, the dispersion relation is solved to yield a critical dynamo number D_c and corresponding critical frequency ω_c as functions of the wavenumber. Dynamo action sets in for $D > D^* \equiv \min_k [D_c(k)]$, with preferred wavenumber $k = k^*$ and corresponding frequency $\omega_c(k^*)$. We shall say that transport hinders dynamo action if increasing the magnitude of γ increases the critical dynamo number D^* , while if D^* is somewhere a decreasing function of γ then transport aids the dynamo instability. The effect of transport on the period of the dynamo wave ($T = 2\pi/\omega_c$), reflecting the time taken to reverse the sign of the magnetic field, will also be investigated, as will its role in modifying the spatial profile of the magnetic field.

Finally, it is also of interest to consider the effect of transport on the phase relation between the radial and azimuthal fields. Observations indicate that $B_r B_\phi < 0$ at active latitudes, i.e. the two components have a phase shift $\phi = \pi$ (see, for example, Stix 1976; Yoshimura 1976; Schlichenmaier & Stix 1995). This phase difference has traditionally been difficult to reproduce with the simplest $\alpha\omega$ -dynamo models that rely upon diffusive communication: given the sign of $\partial\Omega/\partial r$ from helioseismology, the sign of α required for equatorward migration ($\alpha < 0$ in the northern hemisphere, $\alpha > 0$ in the southern) generates poloidal field whose sign is inconsistent with the above phase relation (see Parker 1987; Schüssler 2005). It is therefore of interest to investigate whether more complex $\alpha\omega$ -models can reproduce the observed behaviour. We note that a non-zero phase difference is inherent in the dynamo equations, even for models with spatially coincident generation regions (see Parker 1955, for example). For our dynamo models, the phase difference will be found by examination of the temporal profiles of the azimuthal and radial fields. For example, at $x = z = 0$ we find

$$\Re[B(t)] \sim \cos\left(\frac{2\pi t}{T}\right), \quad \Re\left[\frac{\partial A(t)}{\partial x}\right] \sim \cos\left(\frac{2\pi t}{T} + \phi\right), \quad (9)$$

where ϕ is the phase difference. It is important also to note that the observational evidence for the phase lag arises from the behaviour of the two components of field at the solar surface. Since the toroidal field is created in the tachocline at approximately $0.7R_\odot$ and is subject to complex processes operating throughout the bulk of the convection zone during its rise to the surface, the phase lag is likely to vary with depth. In this investigation we choose to evaluate ϕ at the interface of the convection zone and tachocline ($z = 0$). For the model of infinite extent in z (Model I) this is done owing to the lack of any other preferred location, whereas in the vertically bounded model (Model II) this is done to minimise the role of boundary conditions.

Before turning to the details of the models, it is interesting to note a common characteristic of both models. As can be observed directly from equations (5) and (6), in the large wavenumber limit the evolution is governed by the diffusive term. Thus $D_c \rightarrow \infty$ as $k \rightarrow \infty$. Furthermore, since in this limit the critical dynamo number and corresponding frequency are independent of the magnitude of the transport mechanism, all the stability curves for different magnitudes of γ_1 and γ_2 collapse onto that for $\gamma_1 = \gamma_2 = 0$.

3 MODEL I: SPATIALLY INFINITE DOMAIN

In this section we solve the dynamo equations (5) and (6) in a domain that is unbounded in the z -direction (see Figure 1a), with boundary conditions

$$a(z) \rightarrow 0, \quad b(z) \rightarrow 0 \quad \text{as } |z| \rightarrow \infty, \quad (10)$$

since neither the shear nor the α -effect alone can sustain dynamo action. Following Parker (1993), we seek solutions of the form (7) with

$$b_1(z) = C \exp[-(S + iQ)z], \quad a_1(z) = (F + Ez) \exp[-(S + iQ)z] \quad \text{in } z > 0, \quad (11)$$

and

$$a_2(z) = J \exp[(s + iq)z], \quad b_2(z) = (L + Mz) \exp[(s + iq)z] \quad \text{in } z < 0. \quad (12)$$

Here $C, S, Q, s, q, \sigma, \omega, k$ are real constants, while we allow E, F, J, L, M to be complex. Since our analysis is linear, there exists one arbitrary amplitude, which we take as C . The boundary conditions (10) require that $S > 0$ and $s > 0$. Applying continuity and the jump relations (8) then leads to the relation (see Appendix A)

$$[S + iQ + s + iq] \left[(S + iQ) + \mu^2(s + iq) + \frac{(\gamma_1 - \gamma_2)}{\eta_1} \right] \left[2(S + iQ) + \frac{\gamma_1}{\eta_1} \right] \left[2(s + iq) - \frac{\gamma_2}{\eta_2} \right] = ik^4 \left(\frac{\alpha G}{\eta_1^2 k^3} \right), \quad (13)$$

where

$$S + iQ = -\frac{\gamma_1}{2\eta_1} \pm \frac{1}{2\eta_1} \sqrt{\gamma_1^2 + 4\eta_1(\sigma + i\omega + \eta_1 k^2)}, \quad s + iq = \frac{\gamma_2}{2\eta_2} \pm \frac{1}{2\eta_2} \sqrt{\gamma_2^2 + 4\eta_2(\sigma + i\omega + \eta_2 k^2)}, \quad (14)$$

and $\mu^2 = \eta_2/\eta_1$. In order to satisfy the conditions at infinity, the signs in expressions (14) are to be chosen so that $S > 0$ and $s > 0$. The term in parentheses on the right-hand side of equation (13) is a dimensionless measure of the relative strength of induction to diffusion and is defined as the dynamo number for this problem, i.e. $D \equiv \alpha G/\eta_1^2 k^3$. Without loss of generality, we take $D > 0$. There exist similar solutions for $D < 0$ but they propagate in the opposite direction. Note that, owing to the lack of any physical length scale in this problem, the dynamo number is here defined in terms of the wavenumber k (e.g. Parker 1955). Thus when we consider the effects of transport on the onset of the dynamo instability as a function of wavenumber we consider the dependence of γ on $k^3 D_c \equiv (\alpha G/\eta_1^2)_c$.

We note that in the absence of the γ -effect the model reduces to that of Parker (1993). In the case of uniform diffusion, ($\eta_1 = \eta_2$) equations (13) and (14) then yield

$$\left(\frac{\alpha G}{\eta_1^2} \right)_c = \pm 32k^3, \quad \omega_c = \pm \eta_1 k^2. \quad (15)$$

In what follows we take the $(\alpha G/\eta_1^2)_c > 0, \omega_c > 0$ solutions as our starting point when considering the effects of non-zero transport; i.e., as the magnitude of γ increases, our solutions are smoothly linked to expressions (15) with the positive signs. As discussed earlier, we split the general case into the following subcases.

3.1 Bidirectional transport and uniform diffusion

We begin with the case $\gamma_1 = -\gamma_2 = \gamma$ and $\eta_1 = \eta_2 = \eta$. Relations (13) and (14) then yield

$$\left(\frac{\alpha G}{\eta_1^2} \right)_c = \frac{2}{\eta^3} (\gamma^2 + 8\eta^2 k^2) (\gamma^2 + 4\eta^2 k^2)^{1/2}, \quad \omega_c = \frac{k}{2} (\gamma^2 + 4\eta^2 k^2)^{1/2} \quad (16)$$

It is clear that increasing γ increases both $(\alpha G/\eta_1^2)_c$ and ω_c . Thus transport hinders the onset of the dynamo instability and decreases the time taken to reverse the field polarity. Furthermore, both relations are independent of the sign of γ . Thus, although one may expect the dynamo properties of the two cases $\gamma < 0$ and $\gamma > 0$, representing flux transport towards and away from the interface in both domains, respectively, to be very different, the critical parameters governing the onset of dynamo action are not affected by the direction of flux transport. We believe this unusual property to be a consequence of the infinite extent of the model.

It is noted that the parameters governing the z -structure of the solution are sensitive to the sign of the γ -effect, *viz.* $S + iQ = s + iq = -\gamma/2\eta + \sqrt{\gamma^2 + 4\eta(\sigma + i\omega + \eta k^2)}/2\eta$. As a consequence, the dependence on γ of the phase difference between the azimuthal and radial fields is different for positive and negative γ , as shown in Figures 2(a,b). In the case when transport is directed towards the interface ($\gamma < 0$), the phase lag is increased as $|\gamma|$ increases, while transport away from the interface ($\gamma > 0$) brings the two components of field more in phase.

The structure of the azimuthal and radial fields is illustrated in Figures 2(c,d). As expected, the eigenfunctions are narrower (wider) when transport is towards (away from) the interface.

3.2 Unidirectional transport and uniform diffusion

Given that flux transport towards the interface hinders the excitation of the dynamo instability in exactly the same manner as does transport away from the interface, it appears intuitively unlikely that a unidirectional γ -effect operating throughout the domain will enhance the efficiency of dynamo action. Indeed, in the case $\gamma_1 = \gamma_2 = \gamma$ and $\eta_1 = \eta_2 = \eta$, analytic investigations yield

$$\left(\frac{\alpha G}{\eta_1^2} \right)_c = 32k^3 \left(1 + \frac{\gamma^2}{4k^2\eta^2} \right)^2, \quad \omega_c = \eta k^2 \left(1 + \frac{\gamma^2}{4k^2\eta^2} \right). \quad (17)$$

The dynamo is most easily excited at $k = k_c = |\gamma|/(2\eta\sqrt{3})$, where $(\alpha G/\eta_1^2)_c = 64|\gamma|^3/(3\eta^3\sqrt{3})$. Thus transport again hinders the onset of the dynamo instability. The frequency increases with increasing magnitude of the transport, and the dynamo prefers to generate waves with ever decreasing wavelength ($\lambda = 2\pi/k$).

It may also be shown analytically that at $z = 0$ increasing the magnitude or changing the direction of the transport has no effect on the phase difference between the toroidal and radial fields, as $\phi = \pi/4$ always. Furthermore, since the phase

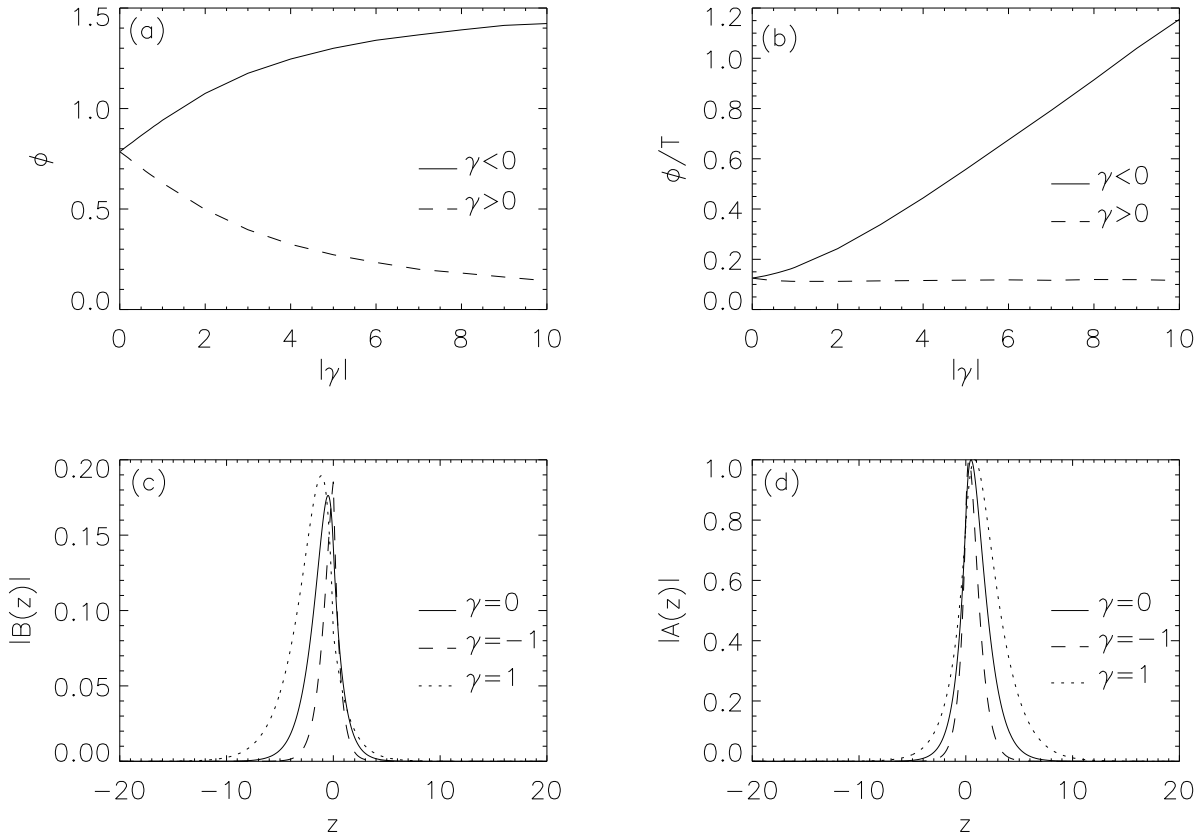


Figure 2. Model I: Bidirectional transport and uniform diffusion ($\gamma_1 = -\gamma_2 = \gamma$, $\eta_2 = \eta_1 = 1$). (a) Phase difference ϕ , (b) Phase difference divided by the period ϕ/T , (c) Toroidal field, (d) Poloidal field. $\gamma = 0$ represents no transport, $\gamma = -1$ transport towards the interface and $\gamma = 1$ transport away from the interface. The eigenfunctions are for $k = 1$ and the phase difference is calculated for $k = 1$ and $x = z = 0$.

relation remains constant even though the critical parameter governing the onset of dynamo action can increase dramatically, the phase lag is not a property that controls the efficiency of dynamo action in the regime studied here.

Figure 3 compares the structure of the azimuthal and radial fields for unidirectional transport directed downwards with that for upwards transport. Downwards transport reduces the decay length of the fields in $z > 0$, while upwards transport reduces the decay length in $z < 0$.

3.3 Dominant transport effect in $z > 0$

We now consider the effects of removing the γ -effect from $z < 0$. In these cases the toroidal field generated in the shear layer will rely upon diffusion to transport it into $z > 0$, where it will act as a source for poloidal field regeneration.

3.3.1 Uniform diffusion

Figures 4(a,b) illustrate the marginal stability curves for the case $\gamma_1 < 0$, $\gamma_2 = 0$ and $\eta_1 = \eta_2 = \eta = 1$. For small wavenumbers

$$\left(\frac{\alpha G}{\eta_1^2}\right)_c \approx \left[\frac{4\gamma_1^8}{\eta^8}\right]^{1/3} k^{1/3}, \quad \omega_c \approx \left[\frac{\eta\gamma_1^2}{2}\right]^{1/3} k^{4/3}, \quad \text{as } k \rightarrow 0, \quad (18)$$

which may be compared with (15) for the case of $\gamma = 0$. Thus, again, transport hinders the onset of dynamo action and increases the frequency of the dynamo waves. It is interesting to note that in comparison with the uniform transport case of §3.2, the removal of the γ -effect from $z < 0$ results in a phase difference that is dependent on the magnitude of γ_1 [Figure 4(c)]. In this case increasing γ_1 increases the phase difference. The ratio of the phase difference to the period of the wave also increases [Figure 4(d)]. The eigenfunctions, shown in Figures 4(e,f), exhibit similar behaviour to the case of a unidirectional transport, with the fields being distorted towards the interface from above (the direction in which the transport operates).

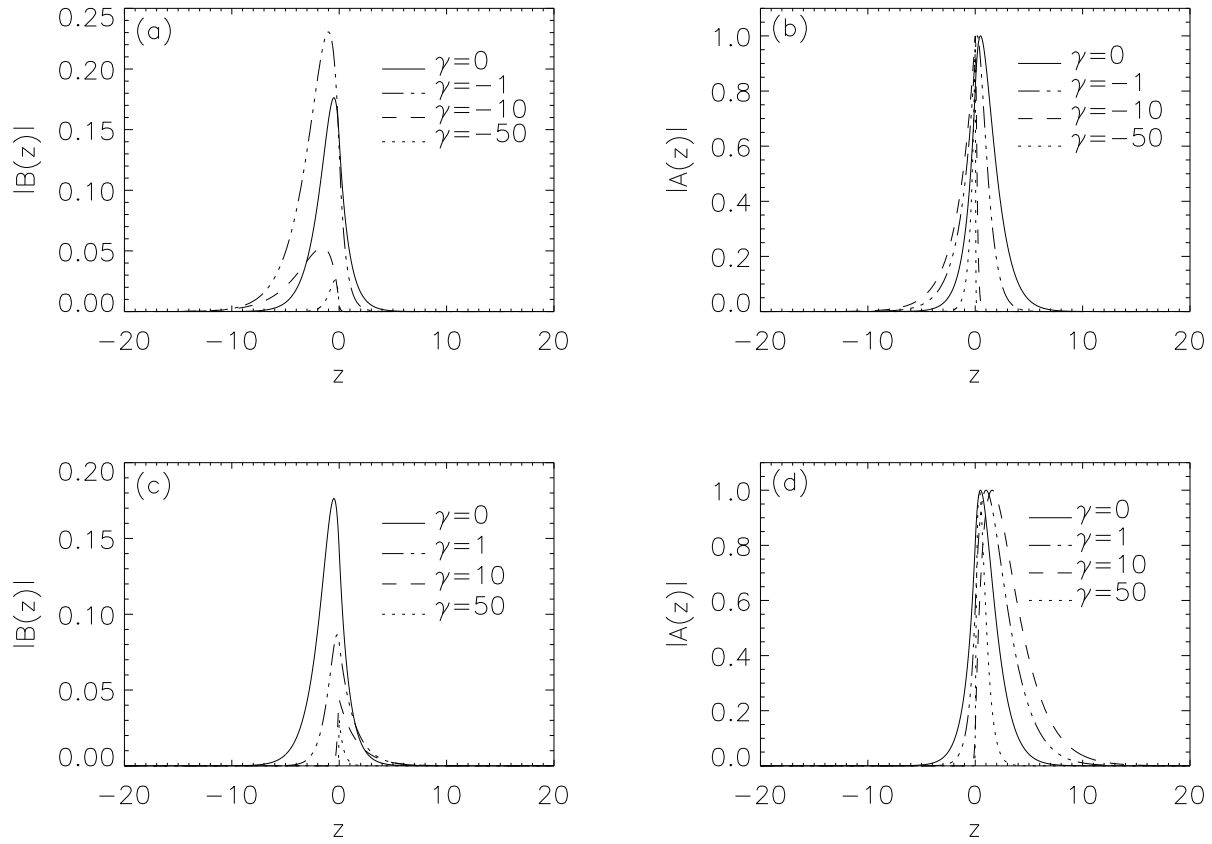


Figure 3. Model I: Unidirectional transport and uniform diffusion ($\gamma_1 = \gamma_2 = \gamma$, $\eta_1 = \eta_2 = 1$, $k = 1$). (a,b) Toroidal and poloidal fields when the γ -effect is directed downwards. (c,d) As for (a,b) with the γ -effect directed upwards. For $\gamma = -50, 10, 50$, the azimuthal field has been multiplied by 10, 50, 1000, respectively.

3.3.2 Reduced diffusion in $z < 0$

The marginal stability curves for the case $\gamma_1 < 0$, $\gamma_2 = 0$, $\eta_1 = 1$ and $\eta_2 = 0.01$ are shown in Figures 5(a,b). Again transport hinders the operation of the dynamo and decreases the period of the dynamo wave. The phase difference between the radial and azimuthal fields behaves in a qualitatively similar manner to the cases investigated above in which the γ -effect is directed downwards, with both ϕ and ϕ/T increasing as the magnitude of γ_1 increases [Figures 5(c,d)]. The behaviour of the eigenfunctions appears to be such that the downwards-directed transport reduces the decay lengths in $z > 0$ [Figures 5(e,f)].

Comparing these results with the uniform diffusion case described above (§3.3.1), one finds that in the absence of γ_1 the dynamo is easier to excite in the case of uniform diffusion than for $\eta_2/\eta_1 = 0.01$, for those wavenumbers considered. Indeed, in the limit $\mu^2 = \eta_2/\eta_1 \rightarrow 0$, Parker (1993), in the absence of transport, derived the relations

$$\left(\frac{\alpha G}{\eta_1^2}\right)_c \approx \frac{2^{5/3}}{\mu^{4/3}} k^3, \quad \omega_c \approx \frac{\eta_1 \mu^{2/3}}{2^{1/3}} k^2, \quad (19)$$

while for $\mu^2 = 1$ we have expressions (15). Clearly, in the absence of non-diffusive transport, $\mu^2 \rightarrow 0$ yields a greater critical dynamo number and a smaller frequency than for the case of uniform diffusion. However, our results reveal that for finite γ_1 the situation is reversed at a certain wavenumber, $k = \tilde{k}(\gamma_1)$, say. For wavenumbers less than \tilde{k} the dynamo is easier to excite in the case with smaller η_2 , while for $k > \tilde{k}$ dynamo action occurs for smaller values of $(\alpha G/\eta_1^2)$ in the case with uniform diffusion. This can be seen by comparing Figures 4(a) and 5(a) for the case $\gamma_1 = -1$, where $\tilde{k}(-1) \approx 0.3$. For those γ_1 considered, the frequencies are larger in the case of uniform diffusion than they are for $\eta_2 = 0.01$. However, it should be noted that for different spatial profiles of γ it is not always the case that uniform diffusion results in a larger frequency (for example, compare the frequencies in Figure 6(b) for $\eta_2 = 1$ and $\eta_2 = 0.01$ in the case of $\gamma_1 = \gamma_2 = -1$). Finally, inspection of the eigenfunctions shows that the reduced η_2 results in a smaller vertical length scale for the toroidal field in $z < 0$, as expected (Parker 1993; Tobias 1996).

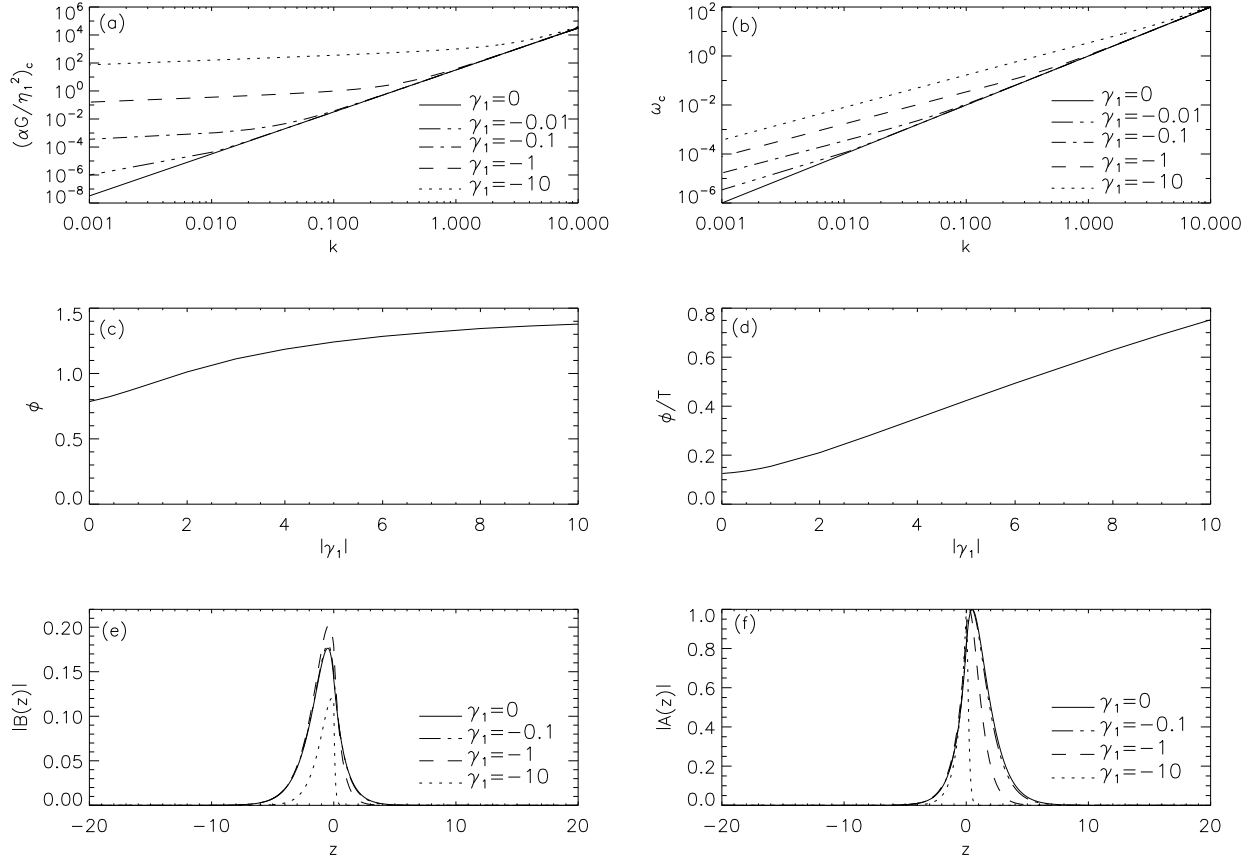


Figure 4. Model I: Dominant transport in $z > 0$ and uniform diffusion ($\gamma_1 < 0$, $\gamma_2 = 0$, $\eta_2 = \eta_1 = 1$). (a) Critical parameter $k^3 D_c$, (b) Critical frequency ω_c , (c) Phase difference ϕ , (d) Phase difference divided by the period ϕ/T , (e) Toroidal field, (f) Poloidal field. The eigenfunctions are for $k = 1$ and the phase difference is calculated for $k = 1$ and $x = z = 0$.

3.4 The competition between the γ -effect and diffusion

It is instructive to consider the effect of varying the diffusivity in $z < 0$ in the absence of the γ -effect and to compare the results with the corresponding situation when γ is non-zero. We consider a fixed value of the wavenumber, here chosen to be $k = 1$, and we take $\gamma_1 = \gamma_2 = \gamma$ for simplicity. Figure 6(a) illustrates that in both cases the effect on $(\alpha G / \eta_1^2)_c$ of varying η_2 is non-monotonic. Decreasing η_2 from unity initially allows a more effective production of toroidal field in $z < 0$ and thus the dynamo becomes easier to excite. However, there exists a transition point ($\eta_2^*(\gamma)$, say) after which decreasing the diffusion hampers the coupling between the two regions sufficiently that the onset of dynamo action is delayed.

Figure 6(b) illustrates that when the γ -effect is absent the frequency decreases monotonically as η_2 decreases, while when $\gamma \neq 0$ there are two distinct regimes. The first is when $\gamma \ll k\eta_2$, in which the frequency of the wave is governed by diffusive transport between the layers. Here the frequency decreases as η_2 decreases. The second regime begins when $k\eta_2$ becomes comparable with γ , and the frequency is then controlled both by diffusion and the γ -effect. As η_2 is decreased further there is an increase in the frequency of the dynamo wave until ω_c eventually saturates at a constant value. In the final state the frequency of the wave is governed by the γ -effect.

Figure 6(c) shows that the phase difference between the toroidal and radial fields is also governed both by diffusion and the γ -effect. The phase difference is typically a non-monotonic function of the diffusion, even for the case $\gamma = 0$. The two components of field initially become more out of phase as the reduced diffusivity favours the generation of toroidal field in $z < 0$. However, as the diffusion is reduced further the phase difference decreases. The ratio of the phase difference to the period of the wave is shown in Figure 6(d).

The effect of reducing the diffusivity in $z < 0$ on the spatial structure of the fields is illustrated in Figures 6(e,f). In the case $\gamma = 0$ (compare Figure 3(a) with 5(e)) the effect of decreasing η_2 is increasingly to confine the toroidal field beneath $z = 0$, as first shown by Parker (1993), while when $\gamma \neq 0$ a sufficiently small diffusion in $z < 0$ allows significant amounts of field to be advected away from the interface.

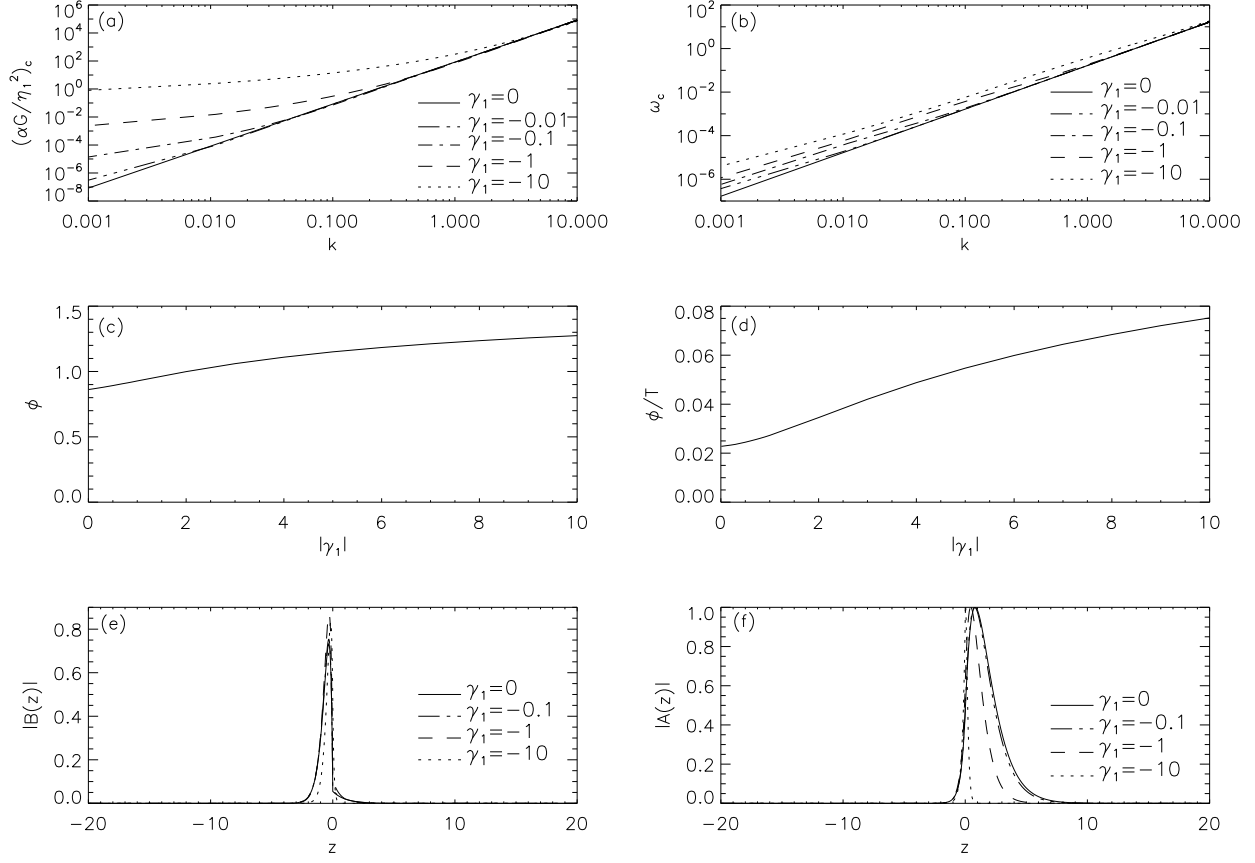


Figure 5. As for Figure 4 with $\gamma_1 < 0$, $\gamma_2 = 0$, $\eta_1 = 1$, $\eta_2 = 0.01$.

4 MODEL II: SPATIALLY CONFINED DOMAIN

In this section we investigate a more realistic model whose vertical extent is limited to $z \in [-L, L]$, where L is finite (see Figure 1b). All other aspects of the geometry remain as in Model I. One consequence of the finite domain is that we may meaningfully non-dimensionalise the system. We let

$$[\mathbf{x}, \alpha, G = \frac{du}{dz}, \eta, \gamma, B, A, t] \equiv [L\mathbf{x}', \alpha_0\alpha', G_0G', \eta_0\eta', \gamma_0\gamma', B_0B', \frac{\alpha_0 L^2 B_0}{\eta_0} A', \frac{L^2}{\eta_0} t'], \quad (20)$$

where primed variables are dimensionless. The dynamo equations then become (dropping the primes)

$$\frac{\partial A_1}{\partial t} = \alpha B + \eta_1 \nabla^2 A_1 - Y_1 \frac{\partial A_1}{\partial z}, \quad \frac{\partial B_1}{\partial t} = \eta_1 \nabla^2 B_1 - Y_1 \frac{\partial B_1}{\partial z} \quad \text{in } z > 0, \quad (21)$$

and

$$\frac{\partial A_2}{\partial t} = \eta_2 \nabla^2 A_2 - Y_2 \frac{\partial A_2}{\partial z}, \quad \frac{\partial B_2}{\partial t} = \eta_2 \nabla^2 B_2 + DG \frac{\partial A_2}{\partial x} - Y_2 \frac{\partial B_2}{\partial z} \quad \text{in } z < 0. \quad (22)$$

Here $Y_{1,2} = R_\gamma \gamma_{1,2}$ is a dimensionless measure of the γ -effect and $R_\gamma = \gamma_0 L / \eta_0$ is its Reynolds number. The dynamo number is defined as $D \equiv \alpha_0 G_0 L^3 / \eta_0^2 > 0$.

Travelling wave solutions of the form (7) are sought in each of $z > 0$ and $z < 0$ and the solutions are matched at the interface $z = 0$ by the jump relations (8). The boundary conditions that approximate the matching onto an external potential field (see Zeldovich, Ruzmaikin & Sokoloff 1983) are,

$$B_1(x, z = 1, t) = 0, \quad \frac{\partial A_1}{\partial z}(x, z = 1, t) = 0, \quad (23)$$

$$B_2(x, z = -1, t) = 0, \quad \frac{\partial A_2}{\partial z}(x, z = -1, t) = 0. \quad (24)$$

The resulting dispersion relation, along with details of its derivation, can be found in Appendix B. Again we split the general case into a number of subcases.

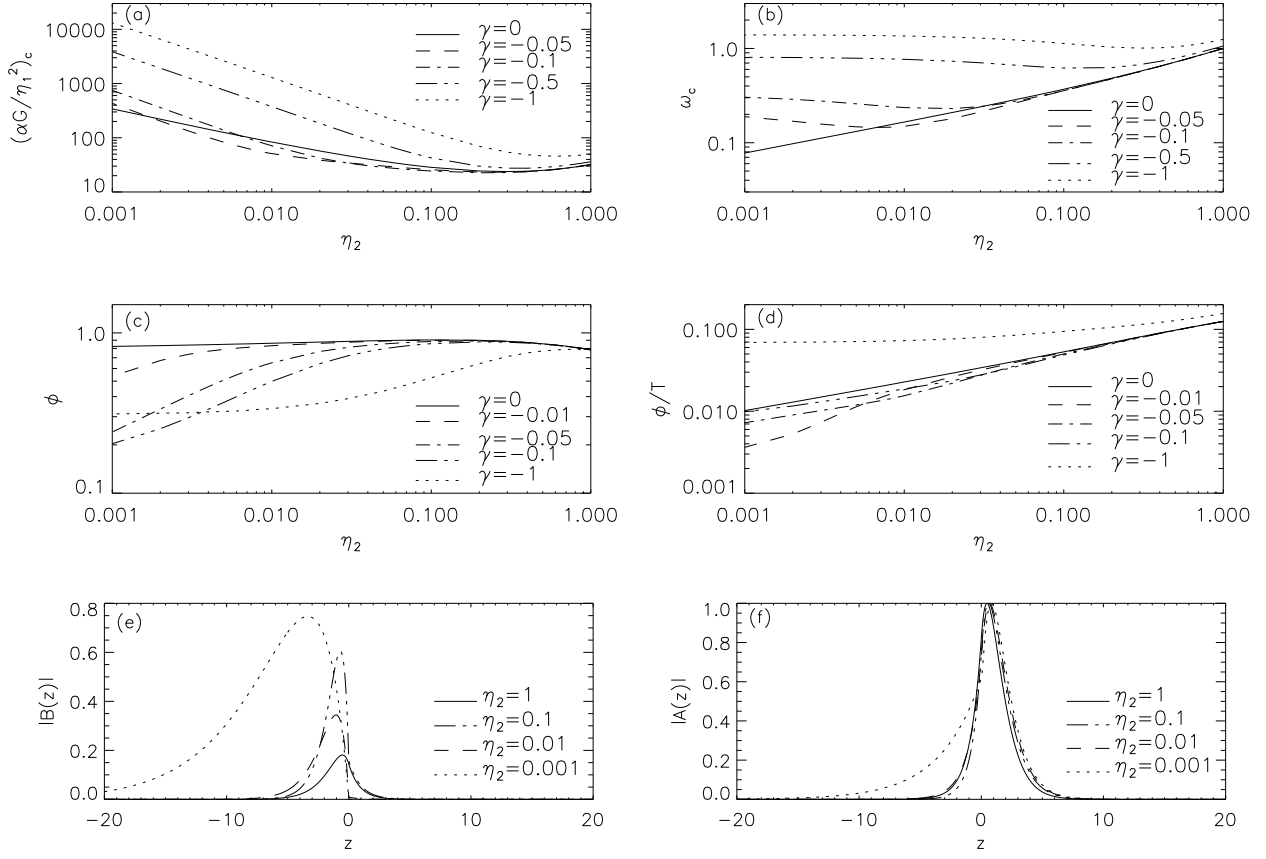


Figure 6. Model I: The competition between the γ -effect and diffusion ($\gamma_1 = \gamma_2 = \gamma < 0$, $\eta_1 = 1$, $k = 1$). (a) Critical parameter $k^3 D_c$, (b) Critical frequency ω_c , (c) Phase difference ϕ , (d) Phase difference divided by the period ϕ/T , (e) Toroidal field, (f) Poloidal field. The eigenfunctions are for $\gamma = -0.05$; for $\eta_2 = 0.01$ and $\eta_2 = 0.001$ the toroidal field has been divided by 10 and 20, respectively. The phase difference is calculated for $x = z = 0$.

4.1 Bidirectional transport and uniform diffusion

It is instructive first to investigate the case in which the γ -effect is directed towards the interface from both above and below. We therefore take $Y_1 = -Y_2 = Y$ with $Y < 0$ and for simplicity we consider the case of uniform diffusion, $\eta_1 = \eta_2 = \eta$. The marginal stability curves and corresponding frequency profiles for different magnitudes of the transport are shown in Figures 7(a,b). For $k \gg 1$, all profiles collapse onto

$$D_c \approx 32 \left(\frac{\eta^2 k^3}{\alpha G} \right), \quad \omega_c \approx \eta k^2, \quad (25)$$

as the system reduces to Model I in the large wavenumber limit (cf. (15); Parker 1993). The numerical results illustrate that the dynamo instability is easiest to excite at $k \ll 1$, where $D_c \approx D_0(Y, \eta)$ and $\omega_c \approx \omega_1(Y, \eta)k$. Analytic investigations for $Y = 0$ yield $D_0(0, \eta) = 16\eta\omega_1$ and $\omega_1(0, \eta) = \eta\sqrt{3/2}$. Figures 7(a,b) illustrate that increasing the magnitude of the transport decreases both D_0 and the corresponding frequency of the dynamo wave. Thus here the transport effect *aids* the onset of the dynamo instability. The time taken for the field to reverse sign increases.

It is interesting that both of the above results concerning the dynamo number and frequency are the direct opposite of any situation that we have previously encountered, i.e. the critical dynamo number and frequency in §3 were increasing functions of γ . In particular, this is true for the corresponding case of Model I (see §3.1), and we are led to the conclusion that boundaries in the z -direction play a crucial role when considering the effects of transport on the efficiency of dynamo action. In fact, investigating the complementary situation in which γ is directed away from the interface in both domains ($Y_1 = -Y_2 = Y$, $Y > 0$) yields numerical results with coefficients D_0 and ω_1 monotonically increasing functions of Y . Recalling that Model I was dependent only on the magnitude of the bidirectional transport mechanism, we conclude that the boundaries in the z -direction cause the model to become sensitive to the direction of flux transport, which is more realistic.

Figures 7(c,d) illustrate the effect of transport on the phase difference between the azimuthal and radial fields, and on the ratio of the phase difference and the period of the wave. For comparison, also presented is the case when transport acts away

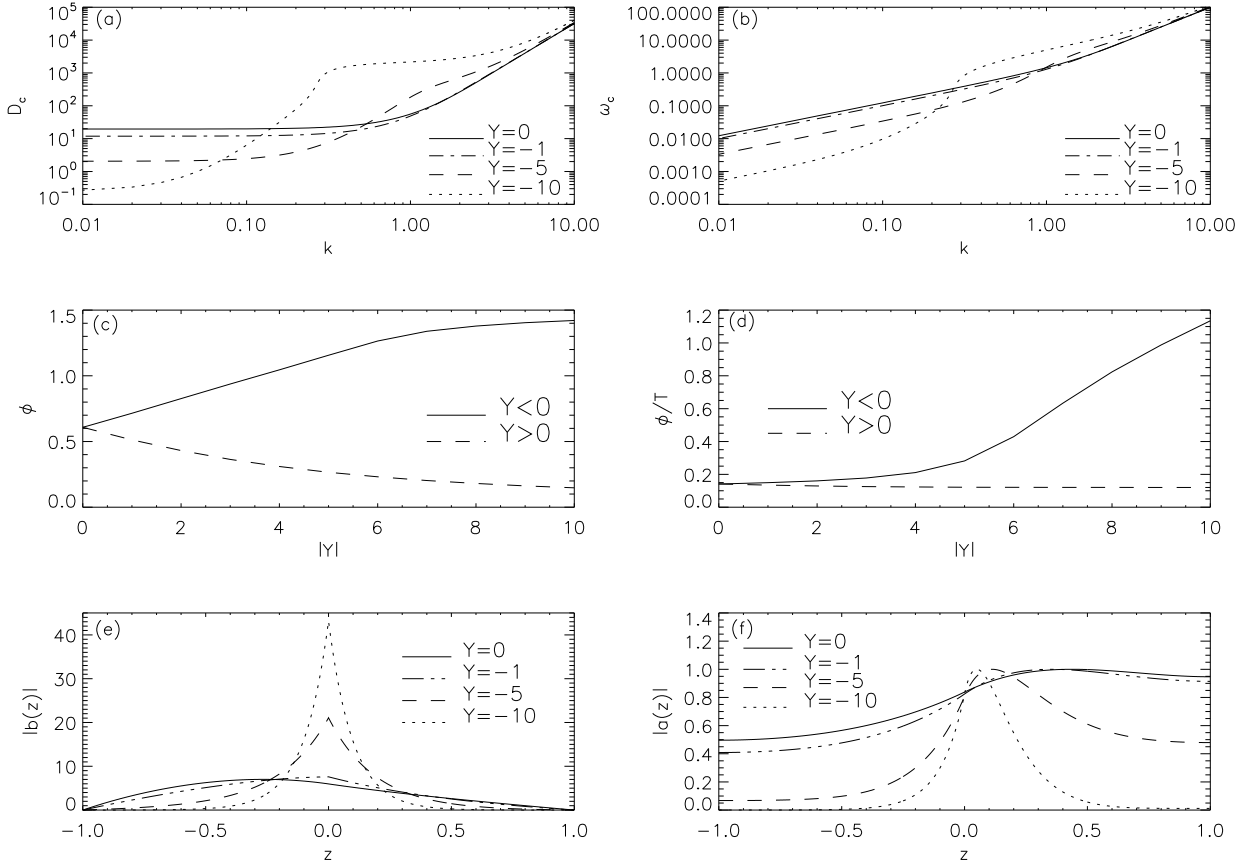


Figure 7. Model II: Bidirectional transport with uniform diffusion ($Y_1 = -Y_2 = Y$, $Y < 0$, $\eta_1 = \eta_2 = 1$). (a) Critical dynamo number D_c , (b) Critical frequency ω_c , (c) Phase difference ϕ , (d) Phase difference divided by the period ϕ/T , (e) Toroidal field, (f) Poloidal field. The toroidal field has been divided by factors of 2 and 4 for $Y = -5$ and $Y = -10$ respectively ($k = 1$). The phase difference and ϕ/T are compared with the case of $Y > 0$ representing transport away from the interface in both $z > 0$ and $z < 0$ ($k = 1$, $x = z = 0$).

from the interface in both regions. Transporting flux towards the interface causes the two components of field to become more out of phase whereas when Y is directed away from the interface the phase difference decreases, in agreement with Model I.

Conveying magnetic flux towards the interface favours field generation there, causing both the toroidal and poloidal fields to become increasingly localised around $z = 0$ [Figures 7(e,f)]. In the contrasting situation of flux transport away from the interface ($Y > 0$) the main effect is to cause the peak in toroidal magnetic field to move towards the lower boundary (behaviour that is qualitatively similar to that shown in Figure 8(e) for uniform downwards transport), whereas there is little change in the z -structure of the poloidal field.

4.2 Unidirectional transport and uniform diffusion

When the transport velocity is uniform throughout the whole domain ($Y_1 = Y_2 = Y$) and the diffusivities are equal, the dispersion relation is independent of the sign of Y . Figures 8(a,b) illustrate that for $k \ll 1$ the critical parameters exhibit different behaviours depending upon the magnitude of the transport: for $|Y| < Y_s(\eta)$, say, the most readily destabilised mode satisfies $D_c \approx D_0(Y, \eta)$, $\omega_c \approx \omega_1(Y, \eta)k$, whereas for $|Y| > Y_s$ we have $D_c \approx D_{-1}(Y, \eta)k^{-1}$, $\omega_c \approx \omega_0(Y, \eta)$ [for $\eta = 1$, $Y_s \approx 3.1$]. Since at large wavenumbers the marginal stability profiles must approach the results (25) for Model I, it follows that for those $|Y| > Y_s$ there exists a preferred wavelength for the dynamo instability (for example, $\lambda^* \approx 2\pi/3$ for $Y = -10$). Figures 8(a,b) illustrate that transport hinders the excitation of the dynamo and decreases the period of the wave.

The phase difference between the azimuthal and radial fields follows a non-monotonic behaviour as the magnitude of Y is increased, and is dependent upon the direction of flux transport [Figures 8(c,d)]. When $Y < 0$ the two fields are most in phase for $Y \approx -1.6$, which can be compared with the situation for $Y > 0$ where the stationary point is a maximum and the fields are most out of phase for $Y \approx 3.2$.

The spatial structure of the toroidal and poloidal fields in the presence of a uniform transport velocity directed towards

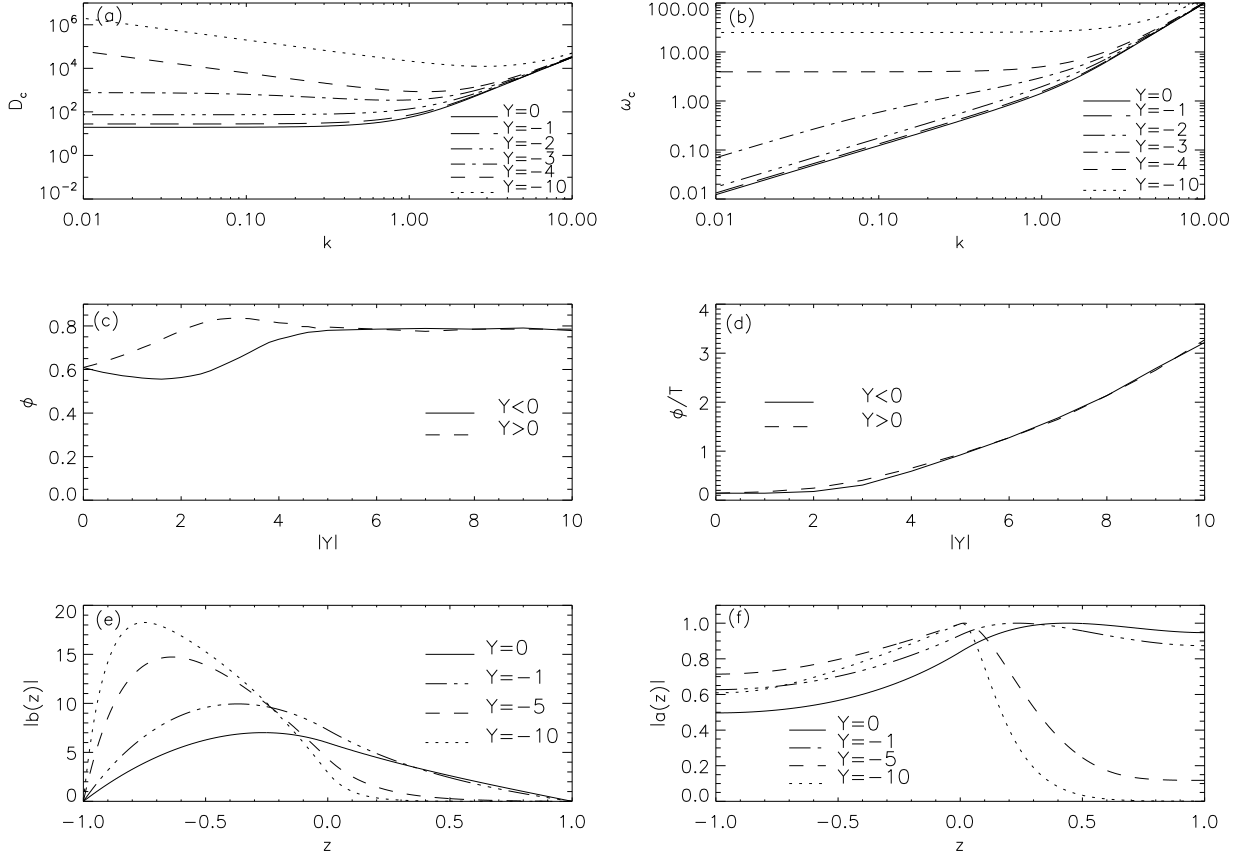


Figure 8. As for Figure 7 with $Y_1 = Y_2 = Y < 0$, $\eta_1 = \eta_2 = 1$. The toroidal field has been divided by factors of 10 and 50 for $Y = -5$ and $Y = -10$ respectively.

the boundary $z = -L$ is shown in Figures 8(e,f). Interestingly, increasing the magnitude of the transport results in the majority of the poloidal field residing in $z < 0$, even though it is generated in $z > 0$.

4.3 Dominant transport effect in $z > 0$

We now consider the case motivated by the Sun, in which the downwards pumping of the convection is much stronger in $z > 0$ than in $z < 0$. We take $Y_2 = 0$ and $Y_1 < 0$ and consider the effects of increasing $|Y_1|$. Flux transport in the tachocline region is then controlled only by diffusion.

4.3.1 Uniform diffusion

We first consider the case of uniform diffusion, $\eta_1 = \eta_2 = \eta$. Figures 9(a,b) show that there is a magnitude of the transport ($Y_{1s}(\eta)$, say) for which there is a qualitative change in the behaviour of the solution at small wavenumbers. This behaviour is similar to the case of a unidirectional γ -effect (see § 4.2) although here the results are dependent on the direction of flux transport. For $\eta = 1$ and $Y_1 < 0$ we have $Y_{1s}(1) \approx -4.9$. For $|Y_1| < |Y_{1s}(\eta)|$ the most readily destabilised mode satisfies $D_c \approx D_0(Y_1, \eta)$ and $\omega_c \approx \omega_1(Y_1, \eta)k$ for $k \ll 1$, while for $|Y_1| > |Y_{1s}(\eta)|$ and $k \ll 1$ we have $D_c \approx D_{-1}(Y_1, \eta)k^{-1}$ and $\omega_c \approx \omega_0(Y_1, \eta)$. Most notably however, and in contrast to all previous calculations, it is found that the minimum of D_c over all wavenumbers as a function of the transport speed Y_1 possesses a stationary value. Thus there exists a preferred magnitude of transport for which dynamo action is most efficient. For $\eta = 1$ the transport that leads to the most efficient dynamo is $Y_1^* \approx -1.2$, where $D_c \approx 16.8$. We shall return to this point in §4.4 [see also Figure 11(c)].

The effect of the transport mechanism on the phase relation between the radial and azimuthal fields is illustrated in Figures 9(c,d). The monotonically increasing behaviour with $|Y_1|$ is similar to that for the same case in Model I (cf. Figures 4(c,d)).

Figures 9(e,f) illustrate the structure of the poloidal and toroidal fields as the transition from transport enhancing to

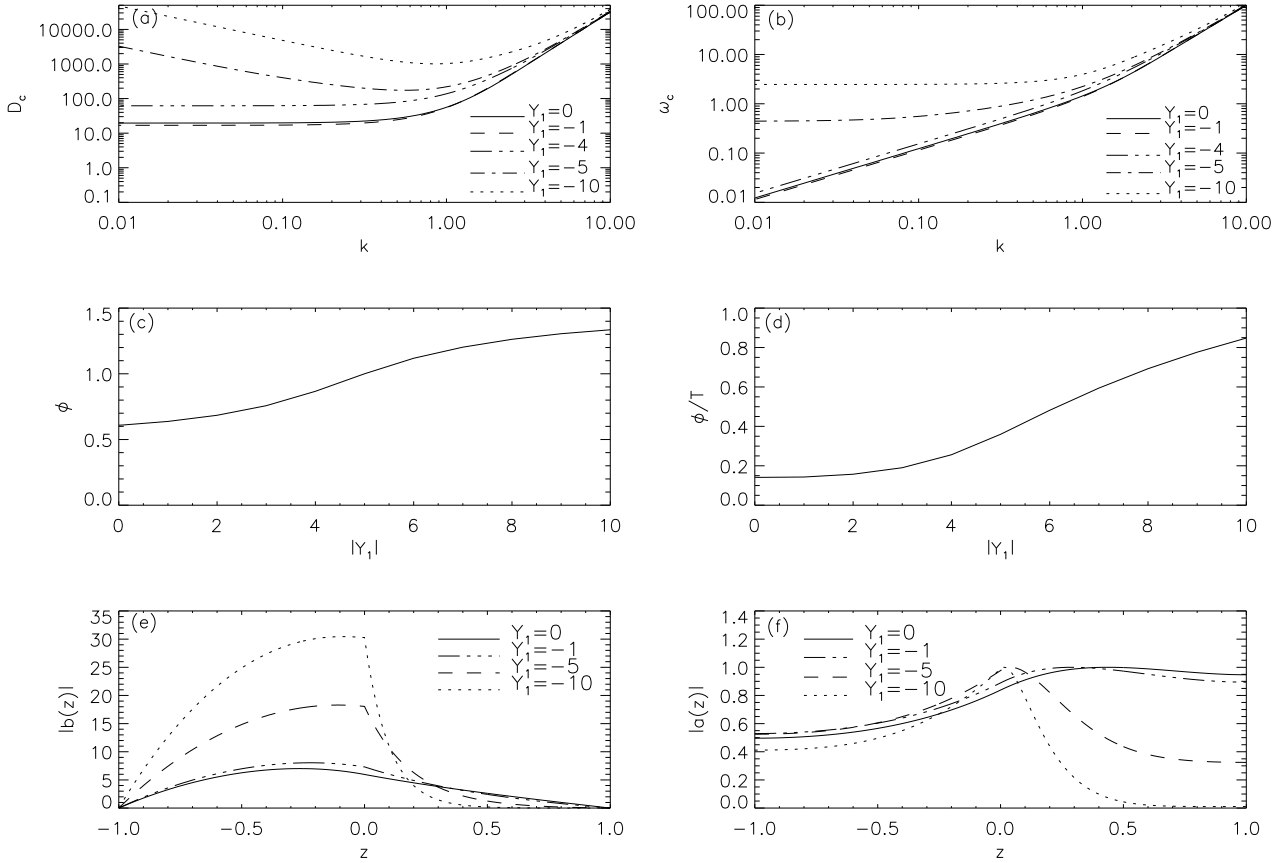


Figure 9. As for Figure 7 with $Y_1 < 0$, $Y_2 = 0$, $\eta_1 = \eta_2 = 1$. The toroidal field has been divided by factors of 2 and 4 for $Y = -5$ and $Y = -10$ respectively.

hindering the dynamo occurs. Although it is difficult to infer from the eigenfunctions alone why a small magnitude of transport helps the dynamo (there appears to be little difference in the spatial profile of the solutions in the cases $Y_1 = 0, -1$), it is interesting to note that in the case when the transport exceeds the preferred magnitude the majority of both the toroidal and poloidal fields resides in $z < 0$. This behaviour is suggestive that Y_1^* corresponds to the strength below which the main effect is to enhance the downwards transport of flux into the tachocline, more readily feeding the ω -effect and leading to more efficient dynamo action, whereas above Y_1^* the diffusive transport of toroidal field into the convection zone is hindered significantly, thus inhibiting the operation of the α -effect and making the dynamo cycle more difficult to complete. Interestingly, the behaviour of the fields in $z > 0$ bears some similarity to the case of a uniform downwards transport throughout the domain [cf. Figures 8(c,d)]. Thus the reason that the dynamo is more difficult to excite in the case of uniform transport (the minima of D_c over all k in Figure 8(a) are greater than those in Figure 9(a)) is likely to be due to the behaviour in $z < 0$: when Y_2 is finite the toroidal field is translated towards the lower boundary where it is annihilated.

4.3.2 Reduced diffusion in $z < 0$

We now consider the case in which the the diffusivity in $z < 0$ is much smaller than that in $z > 0$. We take $\eta_1 = 1$, $\eta_2 = 0.01$ and compare the results with the uniform diffusion case above (§4.3.1). The profiles of the critical dynamo number and corresponding frequency are shown in Figures 10(a,b).

At large values of the wavenumber the profiles collapse onto those for $Y_1 = Y_2 = 0$. Indeed, for $k \gg 1$ and $\mu^2 \rightarrow 0$ the critical dynamo number and frequency are given by the relations (19) (Parker 1993). The numerical results show that for $k \ll 1$, $D_c \approx D_0(Y_1, \eta_1, \eta_2)$ and $\omega_c \approx \omega_1(Y_1, \eta_1, \eta_2)k$, where the coefficients D_0 and ω_1 are non-monotonic in Y_1 . Thus again a preferred magnitude of transport, Y_1^* , exists for which the dynamo is most easily excited. For $\eta_2 = 0.01$ and $Y_1 < 0$, $Y_1^* \approx -6.5$ [see also Figure 11(d)]. It is noted that when transport is absent the dynamo is easier to excite when $\eta_2 = 1$ than when $\eta_2 = 0.01$; however a comparison of the preferred strengths in the two cases (i.e. $D_c(Y_1^* \approx -6.5, \eta_2 = 0.01) = 0.99$

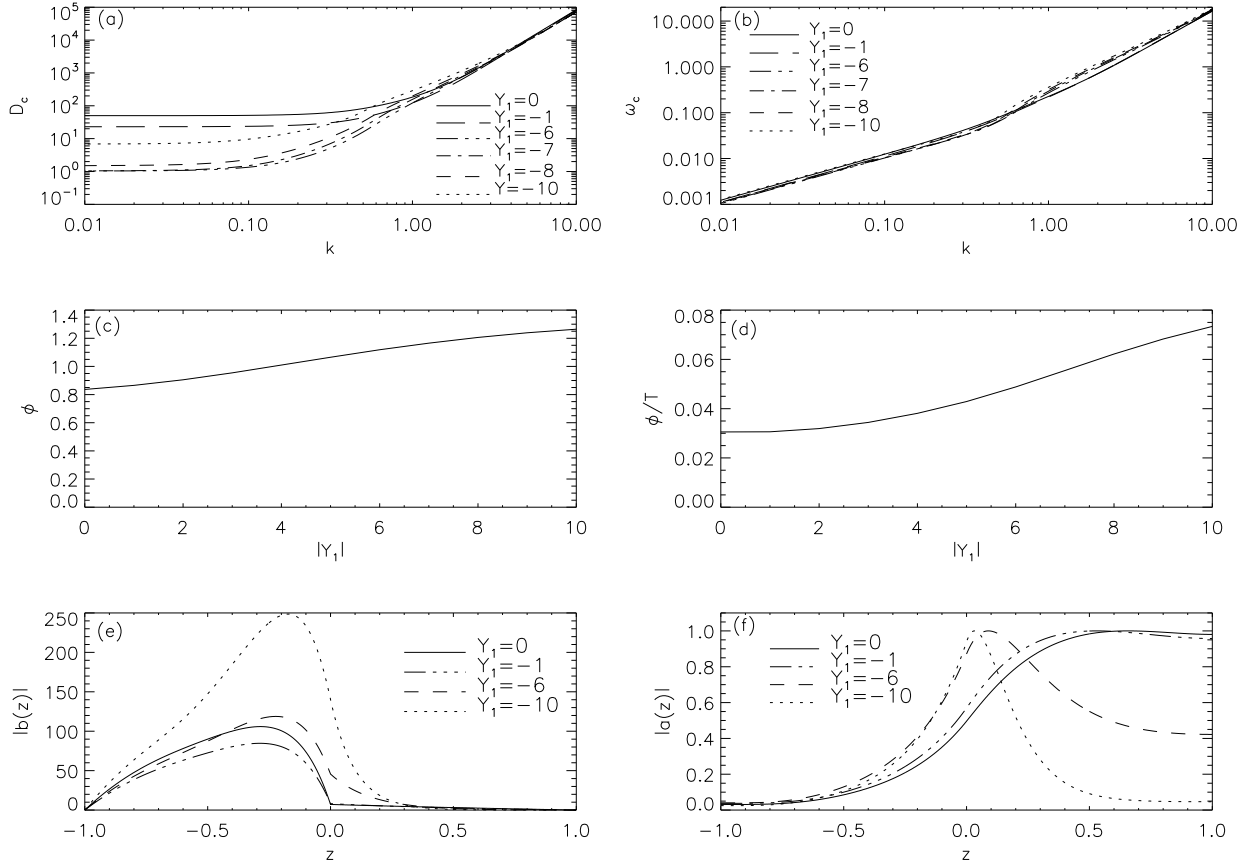


Figure 10. As for Figure 7 with $Y_1 < 0$, $Y_2 = 0$, $\eta_1 = 1$, $\eta_2 = 0.01$.

compared with $D_c(Y_1^* \approx -1.2, \eta_2 = 1) = 16.8$) shows that the stronger γ -effect and smaller diffusivity ratio results in a more efficient dynamo.

The effect of transport on the phase relation between the radial and azimuthal fields, and also the ratio of the phase lag to the period of the wave, is shown in Figures 10(c,d). The behaviour is qualitatively similar to that for the case of uniform diffusion with $Y_2 = 0$ (cf. Figures 9(c,d)).

Figures 10(e,f) illustrate the effect on the eigenfunctions of increasing the transport in $z > 0$. The structure of the toroidal field is affected only weakly, whereas the poloidal field becomes more localised around the interface, the effect being particularly pronounced in $z > 0$.

4.4 The most efficient dynamo

Finally, to summarise the findings for this model and to compare the efficiency of the four cases considered, Figures 11(a-d) present the minimum value of the critical dynamo number over all wavenumbers as a function of the γ -effect for each case. Figure 11(a) illustrates the most efficient dynamo model in which the γ -effect is directed towards the interface from both above and below. Increasing the strength of the γ -effect in this case monotonically decreases the threshold for the dynamo instability. Figure 11(b) illustrates the least efficient dynamo model. In this case a uniform transport mechanism operating throughout the domain hinders dynamo action, with the minimum critical dynamo number increasing monotonically with increasing strength of the γ -effect. Figures 11(c,d) illustrate the cases when the non-diffusive transport is restricted to operate only in $z > 0$, with uniform diffusion in the former and a reduced diffusion in $z < 0$ in the latter. In both of these cases there exists a preferred magnitude of the γ -effect for which dynamo action is most efficient.

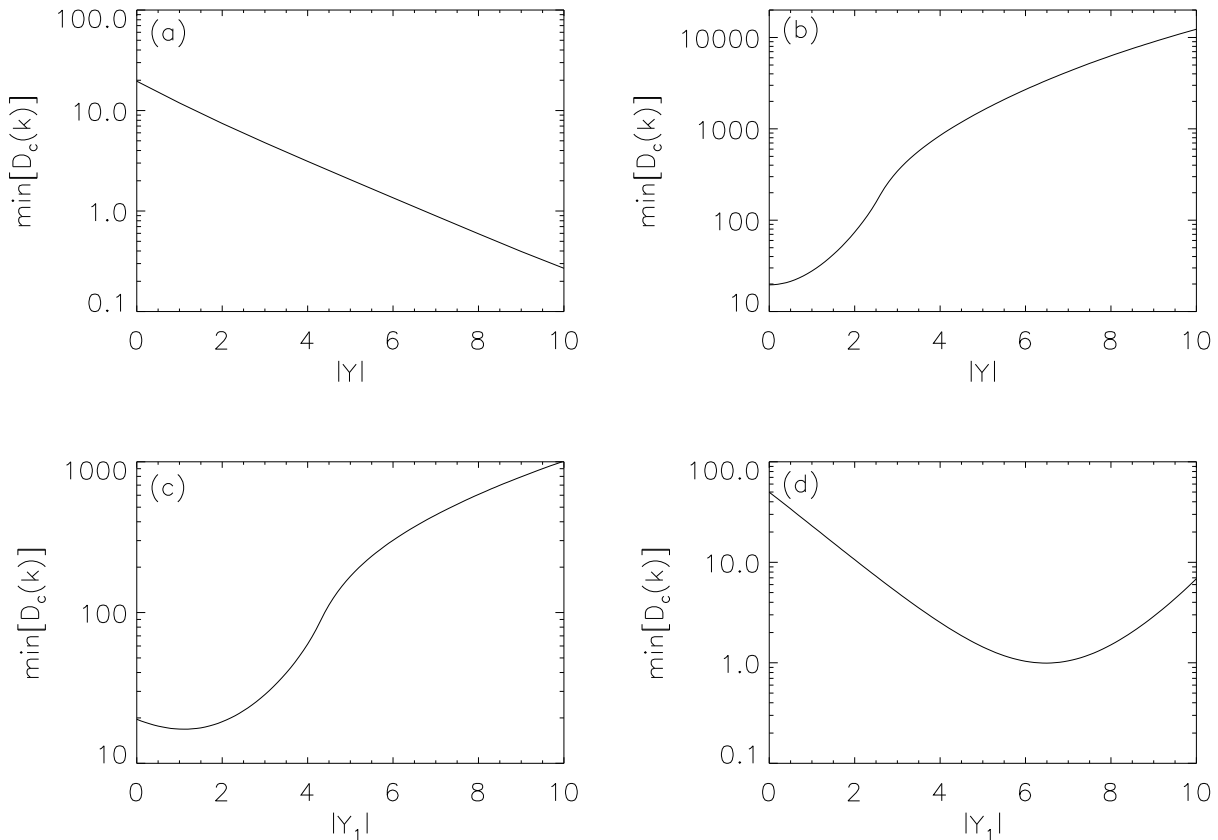


Figure 11. Model II: $\min_k[D_c(k)]$ versus magnitude of transport. (a) Bidirectional transport towards the interface with uniform diffusion ($Y_1 = -Y_2 = Y$, $Y < 0$, $\eta_1 = \eta_2 = 1$), (b) Unidirectional transport and uniform diffusion ($Y_1 = Y_2 = Y$, $\eta_1 = \eta_2 = 1$), (c) Dominant transport in $z > 0$ with uniform diffusion ($Y_1 < 0$, $Y_2 = 0$, $\eta_1 = \eta_2 = 1$), (d) Dominant transport in $z > 0$ with reduced diffusion in $z < 0$ ($Y_1 < 0$, $Y_2 = 0$, $\eta_1 = 1$, $\eta_2 = 0.01$). Cases (c) and (d) have a finite most efficient strength of the γ -effect, $Y_1^* \approx -1.2, -6.5$, respectively.

5 CONCLUSION

We have considered the role of anisotropic transport on the efficiency of an interface dynamo in the linear regime, and its effect in modifying the temporal structure of the solution, through the frequency of the dynamo wave and the phase relation between the radial and azimuthal fields. One of the main findings of the investigation is that the conclusions to be drawn depend crucially upon the geometry of the model.

The first model considered was of infinite vertical extent. In the absence of transport, the preferred wavenumber for the onset of the dynamo instability is $k = 0$, where the critical parameter $(\alpha G/\eta_1^2)_c = 0$. Although, clearly, this cannot be decreased by incorporating the γ -effect, for all forms of transport investigated it is found that $\min_k[(\alpha G/\eta_1^2)_c]$ increases as the magnitude of the transport increases. Thus dynamo action is less readily achieved. Also, the period of the dynamo wave decreases as the magnitude of the γ -effect increases. Thus although the dynamo is more difficult to excite, it more quickly reverses the polarity of the field. Perhaps most noteworthy is that for this model the two cases of the γ -effect directed towards the interface from both above and below and of the transport directed away from the interface in both regions have identical critical dynamo numbers and corresponding frequencies (§3.1).

The effect of the transport mechanism in the more realistic Model II is more complex. The model geometry is the same as that of Model I except that the domain of the problem is bounded in the vertical direction. Here it is found that a uniform transport velocity throughout the convection zone and tachocline delays the onset of the dynamo instability and increases the frequency of the dynamo waves. However, transport directed towards the interface in both $z > 0$ and $z < 0$ decreases both the critical dynamo number and the frequency. Thus transport aids the onset of the instability in this case, although it then takes longer to reverse the field polarity. Restricting the transport mechanism to the convection zone reveals a preferred strength for dynamo action.

It is of interest to relate our studies to previous investigations of the effects of transport on dynamo models. Brandenburg et al. (1993) and Gabov et al. (1996) considered models of galactic dynamos and investigated the role of turbulent diamagnetism

on the dynamo instability via the additional term $\nabla \times (-\nabla\beta/2 \times \mathbf{B})$ in the induction equation, where β is the turbulent diffusivity. Brandenburg et al. (1993) illustrated that a galactic wind can enhance the instability by transporting field into regions of stronger generation, while turbulent diamagnetism can act to oppose this effect and hence hinder dynamo action. Similarly, Gabov et al. (1996) illustrated that the critical dynamo number is larger when the effects of turbulent diamagnetism are present. This was attributed, in part, to an increase in the effective diffusion coefficient. It was then shown that the effective dynamo number $D_c/\tilde{\beta}^2$ (where $\tilde{\beta}$ is the mean value of the turbulent diffusion coefficient) decreases as $\tilde{\beta}$ is increased. It was further illustrated that for highly supercritical dynamo numbers the linear growth rate is larger when turbulent diamagnetism is present than in its absence. In our study we have concentrated on the effects of transport on marginally stable solutions. Nightingale (1983) incorporated the γ -effect into a spherical α^2 -dynamo model and found that the dynamo growth rate is smaller when γ is non-zero than when there is no transport. Rädler (1986) considered spherical $\alpha\omega$ - and α^2 -dynamos and showed that although radial transport mainly hinders dynamo action, certain strengths of γ can promote the instability.

Finally, we remark that interface dynamo models relying purely upon diffusive communication are sometimes rejected owing to their inability to reproduce either the observed direction of propagation of the dynamo belts (exemplified in the butterfly diagram) or the observed phase relation between the radial and azimuthal fields. In this regard, it is of interest to note that the study by Brandenburg et al. (1992) showed that a sufficiently strong downward pumping can lead to an equatorward migration of the magnetic field even when the conventional rule for the sign of $\alpha\partial\Omega/\partial r$ yields a poleward migration. Also, here we have shown that the transport mechanism changes the ratio of the phase difference to the period of the dynamo wave. It is therefore entirely possible that tuning the γ parameter could enable interface dynamo models to reproduce the observed behaviour.

ACKNOWLEDGEMENTS

J.M. was funded by a Ph.D studentship from the EPSRC, UK, and by the NSF sponsored Center for Magnetic Self-Organization at the University of Chicago. The paper was completed at the Kavli Institute for Theoretical Physics, supported by Grant No. NSF PHY05-51164.

APPENDIX A – DISPERSION RELATION FOR MODEL I

In $z > 0$ we seek solutions of the form

$$B_1 = C \exp[t(\sigma + i\omega)] \exp[-z(S + iQ)] \exp(ikx), \quad (26)$$

$$A_1 = (F + Ez) \exp[t(\sigma + i\omega)] \exp[-z(S + iQ)] \exp(ikx), \quad (27)$$

where C, E, F are constants and σ, ω, S, Q, k are real, with $S > 0$ so that $\mathbf{B} \rightarrow 0$ as $z \rightarrow +\infty$. Substitution into equations (5) gives

$$E[2\eta_1(S + iQ) + \gamma_1] = \alpha C, \quad \sigma + i\omega = -k^2\eta_1 + \eta_1(S + iQ)^2 + \gamma_1(S + iQ), \quad (28)$$

with F arbitrary.

In $z < 0$ we look for solutions of the form

$$A_2 = J \exp[t(\sigma + i\omega)] \exp[z(s + iq)] \exp(ikx), \quad (29)$$

$$B_2 = (L + Mz) \exp[t(\sigma + i\omega)] \exp[z(s + iq)] \exp(ikx), \quad (30)$$

where J, L, M are constants and σ, ω, s, q, k are real with $s > 0$ so that $\mathbf{B} \rightarrow 0$ as $z \rightarrow -\infty$. Substitution into equations (6) then gives

$$M[2\eta_2(s + iq) - \gamma_2] = -ikGJ, \quad \sigma + i\omega = -k^2\eta_2 + \eta_2(s + iq)^2 - \gamma_2(s + iq), \quad (31)$$

with L arbitrary. Applying continuity of A and B across $z = 0$, together with the jump conditions (8), yields

$$F = J, \quad C = L, \quad \gamma_2 L - \gamma_1 C - \eta_2 M - \eta_2 L(s + iq) - \eta_1(S + iQ)C = 0, \quad E = F(S + iQ) + J(s + iq). \quad (32)$$

Equations (28a), (31a) and (32) may be combined to yield two equations for C and F . A non-trivial solution requires that the determinant of the coefficients of C and F vanishes, from which we obtain the relation

$$(S + iQ + s + iq) \left((S + iQ) + \mu^2(s + iq) + \frac{(\gamma_1 - \gamma_2)}{\eta_1} \right) \left(2(S + iQ) + \frac{\gamma_1}{\eta_1} \right) \left(2(s + iq) - \frac{\gamma_2}{\eta_2} \right) = ik^4 D, \quad (33)$$

where $D = \alpha G/\eta_1^2 k^3$ and $\mu^2 = \eta_2/\eta_1$. Recall that we also have equations (28b) and (31b) that relate s, q, S and Q to the complex growth rate.

APPENDIX B – DISPERSION RELATION FOR MODEL II

We consider first the convection zone ($z > 0$). The dynamo equations (21), together with the proposed form of solutions (7), yield

$$\frac{d^2 b_1}{dz^2} - \frac{Y_1}{\eta_1} \frac{db_1}{dz} - \frac{q_1^2}{\eta_1} b_1 = 0, \quad \frac{d^2 a_1}{dz^2} - \frac{Y_1}{\eta_1} \frac{da_1}{dz} - \frac{q_1^2 a_1}{\eta_1} = -\frac{\alpha b_1}{\eta_1}, \quad (34)$$

where $q_1^2 = p + \eta_1 k^2$ and $Y_1 = R_\gamma \gamma_1$. Solving equation (34a) for b_1 and applying boundary condition (23a) yields

$$b_1(z) = 2A \sinh[\bar{m}(z-1)] \exp\left(\frac{Y_1(z-1)}{2\eta_1}\right), \quad (35)$$

where A is a constant and $\bar{m} = \sqrt{Y_1^2 + 4\eta_1 q_1^2}/2\eta_1$. Substituting b_1 into equation (34b) and solving the homogeneous equation we obtain

$$a_{1c}(z) = \exp\left(\frac{Y_1(z-1)}{2\eta_1}\right) (C \cosh[\bar{m}(z-1)] + E \sinh[\bar{m}(z-1)]). \quad (36)$$

Looking for a particular solution of the inhomogeneous part of the form

$$a_{1p}(z) = z \exp\left(\frac{Y_1(z-1)}{2\eta_1}\right) (I \cosh[\bar{m}(z-1)] + F \sinh[\bar{m}(z-1)]) \quad (37)$$

we find $I = -\alpha A/\eta_1 \bar{m}$ and $F = 0$. On application of boundary condition (23b) we finally obtain the full solution

$$a_1(z) = \exp\left(\frac{Y_1(z-1)}{2\eta_1}\right) \left(C \cosh[\bar{m}(z-1)] + \left[\frac{A\alpha}{\eta_1 \bar{m}^2} \left(1 + \frac{Y_1}{2\eta_1}\right) - \frac{Y_1 C}{2\eta_1 \bar{m}} \right] \sinh[\bar{m}(z-1)] - \frac{z A \alpha}{\bar{m} \eta_1} \cosh[\bar{m}(z-1)] \right). \quad (38)$$

Following a similar procedure in the tachocline region ($z < 0$), the corresponding equations to (34) read

$$\frac{d^2 b_2}{dz^2} - \frac{Y_2}{\eta_2} \frac{db_2}{dz} - \frac{q_2^2}{\eta_2} b_2 = -\frac{ik D G a_2}{\eta_2}, \quad \frac{d^2 a_2}{dz^2} - \frac{Y_2}{\eta_2} \frac{da_2}{dz} - \frac{q_2^2}{\eta_2} a_2 = 0, \quad (39)$$

where $q_2^2 = p + \eta_2 k^2$, with solutions

$$a_2 = J \exp\left(\frac{Y_2(z+1)}{2\eta_2}\right) \left(\cosh[\bar{n}(z+1)] - \frac{Y_2}{2\eta_2 \bar{n}} \sinh[\bar{n}(z+1)] \right), \quad (40)$$

$$b_2(z) = \exp\left(\frac{Y_2(z+1)}{2\eta_2}\right) \left(\frac{ik D G Y_2 J}{4\eta_2^2 \bar{n}^2} (1+z) \cosh[\bar{n}(z+1)] + \left(L - \frac{ik D G J z}{2\eta_2 \bar{n}} \right) \sinh[\bar{n}(z+1)] \right), \quad (41)$$

where $\bar{n} = \sqrt{Y_2^2 + 4\eta_2 q_2^2}/2\eta_2$. Applying the jump conditions (8) (with γ replaced by Y) and continuity of A and B across $z = 0$ gives four equations for the four unknown constants A , C , J and L . A non-trivial solution requires that the determinant of the coefficients vanishes, from which we obtain the dispersion relation

$$\begin{aligned} & -2(2\eta_2 \bar{n} \cosh[\bar{n}] - Y_2 \sinh[\bar{n}]) \left[i\alpha D G Y_1 Y_2 k \bar{m} \cosh^2[\bar{m}] \cosh[\bar{n}] + \right. \\ & \cosh[\bar{m}] \sinh[\bar{m}] (-i\alpha D G Y_1 Y_2 k \cosh[\bar{n}] + 4\eta_1^2 \bar{m}^2 \bar{n} (-Y_2^2 + 4\eta_2^2 \bar{n}^2) \sinh[\bar{n}]) - \\ & \bar{m} \sinh^2[\bar{m}] \left([i\alpha D G (2\eta_1 + Y_1) Y_2 k + 4\eta_2^2 (Y_1^2 - 4\eta_1^2 \bar{m}^2) \bar{n}^2] \cosh[\bar{n}] \right. \\ & \left. + 2\bar{n} (\eta_1 Y_1 Y_2^2 - \eta_2 Y_2 (Y_1^2 - 4\eta_1^2 \bar{m}^2) - 4\eta_1 \eta_2^2 Y_1 \bar{n}^2) \sinh[\bar{n}] \right) \left. \right] + \\ & \sinh[\bar{n}] \left\{ i\alpha D G (2\eta_2 - Y_2) k (-2(\eta_1 + Y_1) \bar{m} + 2\eta_1 \bar{m} \cosh[2\bar{m}] + Y_1 \sinh[2\bar{m}]) (-Y_2 \cosh[\bar{n}] + 2\eta_2 \bar{n} \sinh[\bar{n}]) \right. \\ & \left. - 4\bar{m} \bar{n} (2\eta_1 \bar{m} \cosh[\bar{m}] + Y_1 \sinh[\bar{m}]) \left[-2\eta_2^2 (Y_1^2 - 4\eta_1^2 \bar{m}^2) \bar{n} \cosh[\bar{n}] \sinh[\bar{m}] + \right. \right. \\ & \left. \left. (-2\eta_1^2 \bar{m} (Y_2^2 - 4\eta_2^2 \bar{n}^2) \cosh[\bar{m}] + (-\eta_1 Y_1 Y_2^2 + \eta_2 Y_2 (Y_1^2 - 4\eta_1^2 \bar{m}^2) + 4\eta_1 \eta_2^2 Y_1 \bar{n}^2) \sinh[\bar{m}]) \sinh[\bar{n}] \right] \right\} = 0 \quad (42) \end{aligned}$$

REFERENCES

- Babcock, H. W., 1961, ApJ, 133, 572
 Brandenburg, A., Moss, D., & Tuominen, I., 1992, in: The Solar Cycle, ed. K.L. Harvey, ASP Conf. Series, 27, 542
 Brandenburg, A., Donner, K. J., Moss, D., Shukurov, A., Sokoloff, D. D. & Tuominen, I., 1993, A&A, 271, 36
 Brandenburg, A. & Subramanian, K., 2005, Phys. Reports, 417, 1
 Cattaneo, F. & Hughes, D. W., 2006, JFM, 553, 401
 Charbonneau, P., & MacGregor, K.B., 1997, ApJ, 486, 502
 Charbonneau, P., 2005, Living Rev. Solar Phys., 2, 2 URL=<http://www.livingreviews.org/lrsp-2005-2>
 Choudhuri, A. R., Schüssler, M. & Dikpati, M., 1995, A&A, 303, L29
 Cline, K. S., Brummell, N. H. & Cattaneo, F., 2003, ApJ, 599, 1449

- Diamond, P.H., Hughes, D.W. & Kim, E.-J., 2005, in *Fluid Dynamics and Dynamos in Astrophysics and Geophysics*, eds. A. M. Soward, C. A. Jones, D. W. Hughes and N. O. Weiss. CRC Press, Boca Raton, FL USA, p.145
- Dikpati, M. & Charbonneau, P., 1999, *ApJ*, 518, 508
- Dikpati, M. & Gilman, P. A., 2001, *ApJ*, 559, 428
- Dikpati, M., Gilman, P. A. & MacGregor, K. B., 2005, *ApJ*, 631, 647
- Dorch, S. B. F. & Nordlund, A., 2001, *A&A*, 365, 562
- Drobyshevski, E. M., & Yuferev, V. S., 1974, *JFM*, 65, 33
- Gabov, A. S., Sokolov, D. D., & Shukurov, A. M., 1996, *Astron. Rep.*, 40, 463
- Hughes, D. W., 2007, in *The Solar Tachocline*, eds. Hughes, D. W., Rosner, R. & Weiss, N. O. Cambridge University Press, p.275
- Hughes, D. W., Rosner, R. & Weiss, N. O., 2007, *The Solar Tachocline*. Cambridge University Press.
- Hughes, D. W. & Cattaneo, F., 2008, *JFM*, 594, 445
- Leighton, R. B., 1969, *ApJ*, 156, 1
- Markiel, J.A., & Thomas, J.H., 1999, *ApJ*, 523, 827
- Moffatt, H. K., 1978, *Magnetic Field Generation in Electrically Conducting Fluids*, (Cambridge: Cambridge Univ. Press)
- Nightingale, S. J., 1983, in *Stellar and Planetary Magnetism*, ed. Soward, A. M. Gordon & Breach Science Publishers, New York.
- Ossendrijver, M., 2003, *A&ARv*, 11, 287
- Parker, E. N., 1955, *ApJ*, 122, 293
- Parker, E. N., 1987, *Sol. Phys.*, 110, 11
- Parker, E. N., 1993, *ApJ*, 408, 707
- Rädler, K.-H., 1968, *Z. Naturforsch.*, 23a, 1851. [English translation: Roberts and Stix, page 267 (1971)]
- Rädler, K.-H., 1986, *Astron. Nachr.*, 307, 89.
- Roberts, P.H. & Stix, M., 1971, *Tech. Note 60*, NCAR, Boulder, Colorado
- Schlichenmaier, R. & Stix, M., 1995, *A&A*, 302, 264
- Schou, J. et al., 1998, *ApJ*, 505, 390
- Schmitt, D., Schüssler, M., & Ferriz-Mas, A., 1996, *A&A*, 311, L1
- Schüssler, M., 2005, *Astron. Nachr.*, 326, 194
- Steenbeck, M., Krause, F., & Rädler, K.-H., 1966, *Zeitschr. Naturforsch.*, 21a, 369 [English translation by Roberts & Stix (1971), page 49]
- Stix, M., 1976, *A&A*, 47, 243
- Thelen, J.-C., 2000, *MNRAS*, 315, 165
- Tobias, S. M., 1996, *ApJ*, 467, 870
- Tobias, S. M., Brummell, N. H., Clune, T. L., & Toomre, J., 1998, *ApJ*, 502, L177
- Tobias, S. M., Brummell, N. H., Clune, T. L., & Toomre, J., 2001, *ApJ*, 549, 1183
- Tobias, S. M., 2005, in *Fluid Dynamics and Dynamos in Astrophysics and Geophysics*, eds. A. M. Soward, C. A. Jones, D. W. Hughes and N. O. Weiss. CRC Press, Boca Raton, FL USA, p.193
- Tobias, S. M. & Weiss, N. O., 2007, in *The Solar Tachocline*, eds. Hughes, D. W., Rosner, R. & Weiss, N. O. Cambridge University Press, p.319
- Yoshimura, H., 1976, *Sol. Phys.*, 50, 3
- Zeldovich, Ya. B., Ruzmaikin, A. A., & Sokoloff, D. D., 1983, *Magnetic Fields in Astrophysics*, (New York, Gordon Breach)